Biogeosciences Discuss., 7, 5269–5304, 2010
www.biogeosciences-discuss.net/7/5269/2010/
doi:10.5194/bgd-7-5269-2010

Biogeosciences Discussions

Satellite observations reveal high variability and a decreasing trend in CO_2 fluxes on the Scotian Shelf

E. H. Shadwick[1], H. Thomas[1], A. Comeau[1], S. E. Craig[1], C. W. Hunt[2], and J. E. Salisbury[2]

[1]Department of Oceanography, Dalhousie University, Halifax, NS, Canada
[2]Ocean Processes Analysis Laboratory, University of New Hampshire, Durham, NH, USA

Received: 24 June 2010 – Accepted: 28 June 2010 – Published: 8 July 2010

Correspondence to: E. H. Shadwick (elizabeth.shadwick@dal.ca)

Published by Copernicus Publications on behalf of the European Geosciences Union.

Abstract

We develop an algorithm to compute pCO_2 in the Scotian Shelf region (NW Atlantic) from satellite-based estimates of chlorophyll-*a* concentration, sea-surface temperature, and observed wind speed. This algorithm is based on a high-resolution time-series of pCO_2 observations from an autonomous mooring. At the mooring location (44.3° N and 63.3° W), the surface waters act as a source of CO_2 to the atmosphere over the annual scale, with an outgassing of $-1.1\,mol\,C\,m^{-2}\,yr^{-1}$ in 2007/2008. A hindcast of air-sea CO_2 fluxes from 1999 to 2008 reveals significant variability both spatially and from year to year. Over the decade, the shelf-wide annual air-sea fluxes range from an outgassing of $-1.7\,mol\,C\,m^{-2}\,yr^{-1}$ in 2002, to $-0.02\,mol\,C\,m^{-2}\,yr^{-1}$ in 2006. There is a gradient in the air-sea CO_2 flux between the northeastern Cabot Strait region which acts as a net sink of CO_2 with an annual uptake of 0.5 to $1.0\,mol\,C\,m^{-2}\,yr^{-1}$, and the southwestern Gulf of Maine region which acts as a source ranging from −0.8 to $-2.5\,mol\,C\,m^{-2}\,yr^{-1}$. There is a decline, or a negative trend, in the air-sea pCO_2 gradient of 23 µatm over the decade, which can be explained by a cooling of 1.3 °C over the same period. Regional conditions govern spatial, seasonal, and interannual variability on the Scotian Shelf, while multi-annual trends appear linked to the North Atlantic Oscillation.

1 Introduction

The rise in atmospheric carbon dioxide (CO_2) from anthropogenic emissions is partially offset by the oceans' CO_2 uptake (Sabine et al., 2004); direct estimates of this uptake require accurate measurements of the partial pressure of CO_2 (pCO_2) in the surface-ocean, and knowledge of its seasonal and interannual variability. Measurements of pCO_2 in the open ocean have become increasingly available (Boutin and Merlivat, 2009; Takahashi et al., 2009; Watson et al., 2009). The increased availability of pCO_2 data has facilitated a deeper understanding of the variability of CO_2 fluxes, particularly

BGD
7, 5269–5304, 2010

for the North Atlantic Ocean (Schuster and Watson, 2007; Thomas et al., 2008; Schuster et al., 2009). These investigations have been complemented by the application of satellite data (Lefèvre et al., 2002; Olsen et al., 2008; Chierici et al., 2009) and modelling studies to respectively increase both spatial and temporal coverage, and to gain a mechanistic understanding of the systems (Etcheto et al., 1999; Wanninkhof et al., 2007; Lefévre et al., 2008; Padin et al., 2008; Thomas et al., 2008). However, while fundamental understanding of air-sea CO_2 exchange in coastal oceans has yet to be achieved, the few available studies provide evidence for highly variable CO_2 fluxes in these regions (Cai et al., 2006; Thomas et al., 2007; Borges et al., 2008). Despite relatively large CO_2 fluxes in coastal oceans (Tsunogai et al., 1999; Thomas et al., 2004), the temporal and spatial variability of pCO_2 remains particularly poorly understood, and the reliability of assessments employing space-borne sensors in these regions has not been established (Cai et al., 2006; Lohrenz and Cai, 2006; Borges et al., 2008; Salisbury et al., 2008).

In the present study we combine highly temporally resolved autonomous observations, in-situ data from monthly shipboard sampling, and space-borne observations to investigate the variability of CO_2 fluxes in the Scotian Shelf region of the Canadian Northwestern Atlantic. The use of these three independent observational techniques allows an assessment of the governing processes at seasonal, interannual, and multi-annual time scales to be made.

2 Methods and data analysis

The seasonal, inter-annual, and multi-annual variability of the CO_2 system on the Scotian Shelf was evaluated using a combination of in-situ autonomous observations from 2007 and 2008, and satellite observations, from 1999 to 2008, for extrapolation in time and space. Hourly, autonomous observations of surface water pCO_2 (µatm), chlorophyll-*a* fluorescence (F_{Chl}), and sea-surface temperature (SST), were made using a CARIOCA buoy moored 30 km offshore from Halifax, at 44.3° N and 63.3° W,

BGD
7, 5269–5304, 2010

between April 2007 and June 2008. Hourly CARIOCA data were uploaded and transmitted daily via the ARGOS satellite system. The pCO_2 measurements were made by an automated spectrophotometric technique (Bates et al., 2000; Bakker et al., 2001; Copin-Montégut et al., 2004). A Sea-Bird (SBE 41) conductivity and temperature sensor was used to measure temperature (°C) and to determine salinity; chlorophyll-*a* fluorescence ($\mu g\,l^{-1}$) was determined by a WET Labs miniature fluorometer (WETstar).

Non-photochemical effects that are related to the intensity of the incoming solar radiation may decrease F_{Chl} up to 80% during the day (Kiefer, 1973). This effect can be avoided by using night-time data which, to a large extent, are free of the effects of non-photochemical quenching, for fluorometer calibration. Night-time data were taken as a mean F_{Chl} between 03:00 and 06:00 UTC; data points were temporally interpolated to match discrete chlorophyll-*a* measurements, Chl-*a* ($mg\,m^{-3}$), from monthly or twice-monthly occupations at the mooring site. A linear regression (r^2=0.76, N=29, p<0.001) was used to determine the relationship between the F_{Chl} and Chl-*a*, and applied to the CARIOCA fluorescence-derived chlorophyll-*a* time-series – Chl_F ($mg\,m^{-3}$), see Table 1 for a summary of notation used to distinguish between the time-series of chlorophyll-*a*).

Wind speed ($m\,s^{-1}$) and atmospheric CO_2 (µatm) were measured hourly by Environment Canada at the Sable Island Meteorological Station (43.9° N and 60.3° W) at a height of 10 m using a sonic anemometer and an open-path infra-red CO_2 analyser. Monthly mean values of pCO_2, Chl_F, and SST, were computed from the CARIOCA time series, comprising more than 2000 observations over a 14 month period. Monthly integrals of the gas transfer velocity, k ($cm\,h^{-1}$), were computed from hourly winds and the formulation of Wanninkhof (1992).

A multiple linear regression (Eq. 1) was applied using monthly mean values of pCO_2, Chl_F, SST, and the gas transfer velocity, k, as predictor variables (i.e. N=14). The regression was also applied to the hourly (night-time) observations (n=2000), and the resulting regression coefficients were similar to those presented in Eq. (1). The choice of monthly means to generate Eq. (1) was made for temporal consistency with the

BGD
7, 5269–5304, 2010

remotely-sensed data obtained on a monthly timescale which was used, along with Eq. (1) to compute pCO_2, and is described in Sect. 2.1. The April value of Chl_F acted as a leverage point, dominating the regression, and allowing the pCO_2 minimum to be reproduced by the model. During the remainder of the year, pCO_2 is influenced to a lesser degree by Chl_F, and more strongly by the annual cycle of SST.

$$pCO_2 = 354.4 - 24.6Chl_F + 4.6SST + 3.7k \quad (1)$$

$$X_t = \frac{1.7}{12}\Delta t \quad (2)$$

Surface water pCO_2 on the Scotian Shelf was reconstructed from January 1999 to December 2008 using Eq. (1). A correction term, X_t (µatm) (Eq. 2), was applied to account for the rise of surface ocean pCO_2 of approximately 1.7 µatm yr^{-1}, relative to January 1999, due to the uptake of anthropogenic atmospheric CO_2 (Thomas et al., 2008). This term is added to the right hand side of Eq. (1) for each month "t", with Δt (months) equal to the number of months since January 1999. For example, in February 1999, X_t would be computed with: $X_t = (1.7/12)$ µatm. The multiple linear regression (Eq. 1) is applied to absolute values of Chl_F, SST, and k, to compute monthly, values of pCO_2. This approach allows the use of predictor variables that can be observed remotely, and captures the underlying physical and biological mechanisms in the system.

Further information regarding the predictive capacity of Chl_F, SST, and k to estimate pCO_2 was gained by computing the z-scores for each of the coefficeints, thereby making them dimensionless and directly comparable. The z-score, or β coefficients are obtained by:

$$z = \frac{(x - \mu)}{\sigma}, \quad (3)$$

where x is the quantity of interest (i.e. pCO_2, Chl_F, SST, or k), μ is the mean value of x, and σ is the standard deviation of x. The magnitude of the β coefficients then allows a direct comparison of the relative contribution, or weight, of each of the predictor

BGD
7, 5269–5304, 2010

variables (i.e. Chl_F, SST, and k) in the estimate of pCO_2 (Table 2). It can be seen from the magnitude of the β coefficients that the Chl_F makes the strongest contribution, and that both the Chl_F and SST coefficients are roughly double the magnitude of the k coefficient.

2.1 Spatial extapolation and validation

Seven 2°×2° grid boxes, covering the Scotian Shelf were defined (Fig. 1). The regression (Eq. 1) was used to generate a hindcast of pCO_2 that was extrapolated spatially using monthly means of satellite-derived chlorophyll-*a* concentration, Chl_{SAT} ($mg\,m^{-3}$), and SST, along with the gas transfer velocity (k) computed with locally measured wind (Fig. 2). The estimates of Chl_{SAT} were acquired from the Level 3 equal-area 9-km data from the Sea-viewing Wide Field-of-view Sensor (SeaWiFS) on the SeaStar platform, while SST was acquired from the Pathfinder AVHRR equal-area 9-km best-SST data product. The monthly Chl_{SAT} data were regressed against the (night-time calibrated), monthly mean, CARIOCA Chl_F timeseries, (r^2=0.68, N=14, p<0.002) and scaled accordingly. The relationship between Chl_F and Chl_{SAT} was roughly 1:1; the satellite derived mean chlorphyll estimate (over the 2°×2° grid box) was in good agreement with the data from the CARIOCA fluorometer. The standard deviation for Chl_{SAT} concentration within a box (containing 576 pixels) ranged from 0.1 to 0.49 $mg\,m^{-3}$, with higher variation in the nearshore boxes. The mean seasonal cycles of SST and pCO_2 were computed using the mean value for each month over the ten-year period (i.e. mean of all January values, mean of all February values, etc.). The SST and ΔpCO_2 anomalies were defined as the deviation from the mean seasonal cycle.

The values of pCO_2 computed from Eq. (1) are compared with pCO_2 measured by the CARIOCA buoy in 2007 and 2008 (Fig. 3). The computed pCO_2 (Eq. 1) are also validated against measurements of pCO_2 made by a continuous flow equilibration system (LiCor, see for example Körtzinger et al., 1996 for a description of the method)

BGD
7, 5269–5304, 2010

in April, August, and October 2007, and April 2008 (Fig. 4). The underway measurements were obtained on monitoring cruises on the Scotian Shelf (see Shadwick et al., 2010, for details of the field program). On the same cruises, discrete sea-water samples were collected at the surface and concentrations of dissolved inorganic carbon (DIC) and total alkalinity (TA) were determined (see Shadwick et al., 2010, for details). Values of surface pCO_2 were computed from DIC and TA using the standard set of carbonate system equations and the program of Lewis and Wallace (1998). The pCO_2 measurements from the underway system, and from the discrete DIC and TA samples are shown in Fig. 4. These observed data represent mean values within a given $2^{\circ}\times2^{\circ}$ grid box over 12 to 36 h, depending on the length of time the ship spent in a given box during the cruise. The different timescales of the computed (monthly) and measured (daily) pCO_2 hinder a direct comparison. However, the agreement between the observed and computed pCO_2 supports the spatial extrapolation of the regression (Eq. 1). The regression overestimates the April pCO_2 compared to the observations made by the CARIOCA buoy in both 2007 and 2008 (Fig. 3). The spatial variance of the of the satellite-derived Chl-*a* (Chl_{SAT}) was particularly high near the location of the CARIOCA mooring in April 2007 (Fig. 1). The pCO_2 measured by the CARIOCA buoy is an average of hourly values over one month in an area that experienced particularly high concentrations of Chl-*a* in April 2007. The computed pCO_2 relies on Chl_{SAT} that has been both spatially and temporally averaged, which may explain the discrepancy between the peak values, seen for example in April. A ten-year time series of discrete Chl-*a* measurements from the mooring location (Fig. 2a inset) indicates much higher concentrations than the Chl_{SAT} time-series used to predict pCO_2 (Fig. 2a and d). However, these data are not monthly mean values, but once-per-month measurements that are expressly biased to produce snapshots of the dominant features of the system, most notably the spring Chl-*a* maximum, corresponding to the annual pCO_2 minimum. The April cruise on the Scotian Shelf is similarly biased; sampling takes place at the height of the bloom. The computed pCO_2 represensts a monthly average, and the peak values are thus smoothed compared to the short-term ship-board observations.

BGD
7, 5269–5304, 2010

The computed pCO_2 reproduces very well the regional summer and autumn concentrations. There is good agreement between the computed pCO_2 and the underway and DIC/TA based measurements in both August and October in all grid boxes (Fig. 4).

2.2 Air-sea CO_2 flux

The air-sea CO_2 fluxes, F (mol C m^{-2} $month^{-1}$), were computed via:

$$F = k\alpha\Delta pCO_2, \quad (4)$$

where α is the coefficient of solubility (Weiss, 1974) and ΔpCO_2 is the gradient in pCO_2 between the ocean and the atmosphere, and the gas transfer velocity (k) was computed using hourly winds (Wanninkhof, 1992) measured at Sable Island. It has been shown that the winds at Sable Island are representative of the winds over the Scotian Shelf (Petrie and Smith, 1977); values of k computed from Sable Island winds were therefore used in the flux computations in each grid box. A negative flux indicates a transfer from the ocean into the atmosphere. Annual flux estimates between different years are compared with the same high precision, as the values of ΔpCO_2, which is essential for a reliable assessment of interannual variability. The accuracy of the flux computations is however lower (20%) due to the large error associated with the gas transfer parameterization (Naegler et al., 2006; Sweeney et al., 2007; Watson et al., 2009).

3 Interpretation of regression coefficients

On the Scotian Shelf the spring bloom occurs coincident with the SST minimum allowing the effects of temperature and biology to be clearly distinguished (Shadwick et al., 2010). The value of the Chl_F regression coefficient obtained in Eq. (1), −24.6 µatm (mg m^{-3})$^{-1}$, is dominated by the spring bloom, and is consistent with a value obtained in a recent regression study in the North Atlantic south of Greenland (Chierici et al.,

BGD
7, 5269–5304, 2010

2009). The Chl_F coefficient corresponds to a ratio of inferred net inorganic carbon assimilation to accumulated chlorophyll in the range of 115 mg C (mg chl-*a*)$^{-1}$, that is higher than literature values of ~50 mg C (mg chl-*a*)$^{-1}$ (Platt et al., 1991). This difference may be explained by the fact that the literature C:Chl-*a* ratios do not account for losses of chlorophyll both due to sinking – whereby chlorophyll leaves the system but the inorganic carbon deficit remains – and grazing leading to the accumulation of detritus and heterotrophic biomass (Weeks et al., 1993; Banse, 1995; Taylor et al., 1997).

The SST regression coefficient obtained in Eq. (1) (4.6 µatm °C^{-1}) is lower than the thermodynamically expected value, which would be roughly 16 µatm °C^{-1} at 400 µatm (Takahashi et al., 2002). This coefficient comprises the effects of temperature, as well as other factors with timing closely tied to the seasonal evolution of temperature, and is discussed in more detail in Sect. 3.1

The gas transfer velocity (k) here serves as a directly assessable representation of the mixed-layer depth. Mixed-layer depth, estimated from monthly profiles of temperature and salinity at the mooring station, is plotted versus monthly values of gas transfer velocity for the year 2008 in Fig. 5. A linear regression revealed a significant correlation between the two variables (r^2=0.79, N=12, p<0.001). By using k, stronger winds, and a deeper mixed-layer, make a large contribution to the monthly value of pCO_2, while weaker winds, and a shallow mixed-layer, make a smaller, though still positive contribution to pCO_2. Mechanistically, with increasing winds, k represents the deepening of the mixed-layer in autumn and winter, which implies an intrusion of CO_2 rich subsurface water into the surface-layer. On the other hand, in spring and particularly in summer, weak winds, and thus lower values of k, yield lower values of pCO_2. In summer, if the moderate biological activity is confined to a shallower mixed-layer, it has a stronger impact on the pCO_2 (or the CO_2 concentration), than if it occurred within a deeper mixed-layer. In the regression model presented here, the k coefficient thus helps assign a third dimension to the areal, two-dimensionally acquired, satellite view. This is required to parameterise the CO_2 concentration changes as driver of the air-sea CO_2

BGD
7, 5269–5304, 2010

flux rather than changes in the CO_2 inventory. The effect of gas exchange itself plays a subordinate role in altering water column CO_2 concentrations on the short, monthly, time scales applicable here.

The change in pCO_2 due to each of the predictor variables was computed using Eqs. (4)–(6), using the 12 monthly mean values of Chl_F, SST and k (Fig. 6). For example, the change in pCO_2 due to chlorophyll, $pCO_2(Chl_F)$, was computed (Eq. 3) by keeping SST and k constant, at their initial, January 2008, values (subscript "J"), and allowing Chl_F to vary. The change in pCO_2 due to SST and k were similarly computed.

$$pCO_2(Chl_F)=354.4+24.6Chl_F+4.6SST_J+3.7k_J \quad (5)$$

$$pCO_2(SST)=354.4+24.6Chl_{FJ}+4.6SST+3.7k_J \quad (6)$$

$$pCO_2(k)=354.4+24.6Chl_{FJ}+4.6SST_J+3.7k \quad (7)$$

The influence of Chl_F (Fig. 6 in green) dominates the total change (in black) in April, and plays a more minor, though non-zero, role during the rest of the year, reflecting the contribution of the late summer, production. The SST control (Fig. 6 in red) increases pCO_2 from April to September, decreases pCO_2 from September to December, and is near neutral from December to April. The gas transfer velocity (Fig. 6 in blue) acts to increases pCO_2 most strongly in the autumn and winter when wind driven mixing enhances the entrainment of high-carbon water into the surface layer.

3.1 Temperature coefficient

A detailed analysis of the time series, paying particular attention to the relationship between pCO_2 and SST, in the frequency domain facilitates an understanding of the deviation of the temperature coefficient ($4.6\,\mu atm\,^{\circ}C^{-1}$) in the regression (Eq. 1) from the expected thermodynamic value. Using a frequency analysis, we decomposed the temperature coefficient into genuine thermodynamic temperature effects, and effects with timing correlated to temperature, which are also encompassed by the SST coefficient.

BGD
7, 5269–5304, 2010

We computed the cross-spectrum of pCO_2 and SST in order to examine the strength of the relationship between these two parameters over a range of frequencies; the gain in pCO_2 due to SST is plotted in Fig. 7a (in blue). The dominant energies in the pCO_2-temperature relationship are found at frequencies, f, $\leq 0.04\,h^{-1}$, and corresponding to periods of $P \geq 24$-h. At the daily frequency, $f = 0.04\,h^{-1}$, (highlighted by pale blue vertical bar in Fig. 7a), the gain has a value of approximately 16 µatm °C^{-1}, which is what the thermodynamic relationship between pCO_2 and temperature predicts (a 4% change in pCO_2 for a 1 °C change in temperature (Takahashi et al., 2002), with a mean annual pCO_2 of roughly 400 µatm). Mechanistically, this is caused by the fact that the seasonal variability of temperature on the Scotian Shelf is primarily driven by surface heat fluxes (Umoh and Thompson, 1994), reflected here by the dominance of SST controlling the daily variability in pCO_2. At frequencies less than $f = 0.04\,h^{-1}$, or for periods longer than 24-h, the temperature related gain in pCO_2 tends away from the thermodynamic value, towards the lower value (4.6 µatm °C^{-1}) obtained in the regression presented here (Eq. 1).

To evaluate the effects correlated with temperature outside of the diurnal cycle, the daily, or 24-h, cycle was removed from the SST time series. This was done by computing the mean temperature over a given, discrete 24-h period, starting at midnight, and subtracting this value from each hourly value of SST over the same period:

$$SST_{(in\text{-}situ)} - SST_{(dailymean)} = \Delta SST^{*} \quad (8)$$

This daily cycle in SST was subsequently removed from the pCO_2 time series via the following equation:

$$pCO_2^{*} = pCO_2 - (pCO_2[\exp(0.0423 \Delta SST^{*})]) \quad (9)$$

where the second term on right-hand side of the equation is the temperature correction of Takahashi et al. (2002), and the superscript * indicates the time series with the 24-h cycle removed.

The gain in pCO_2^{*} due to SST* is shown in Fig. 7a (red dashed line). The energy of the daily frequency has vanished to a large degree ($f = 0.04\,h^{-1}$, highlighted by the pale

BGD
7, 5269–5304, 2010

blue vertical bars in Fig. 7), and the temperature correlated pCO_2^* gain at $f=0.02\,h^{-1}$, which correspond to periods shorter than roughly 40 h, (highlighted by the pink vertical bars in Fig. 7), lies between 4 and 6 µatm °C^{-1} which is consistent with the SST coefficient obtained in the regression (Eq. 1). The dominant gain in the temperature corrected pCO_2 data however is now observed at a frequency of $f=0.007\,h^{-1}$, (highlighted by the green vertical bars in Fig. 7), corresponding to periods from several days to a month. The gain at this frequency is 13 µatm °C^{-1}, with a phase lag of roughly 180 degrees (highlighted by the green vertical bars in Fig. 7b), or −13 µatm °C^{-1}, and can be attributed to biological CO_2 uptake, with seasonal cycle strongly anti-correlated to that of temperature. This anti-correlation has been confirmed by Shadwick et al. (2010), by employing an alternate 1-D modelling approach (see Fig. 8 inset). Furthermore, a linear regression of the temperature corrected pCO_2 data with in-situ temperature, as shown by Shadwick et al. (2010) (their Fig. 8), yields a coefficient of −13 µatm °C^{-1}, as described above.

In general, the regression coefficient obtained is thus composed of the competing influences of the thermodynamic temperature dependence of pCO_2, and the pCO_2 dependence on biological processes. The net effect of these two processes is captured in the regression model presented here. At monthly time scales, the regression yields an SST coefficient encompassing the thermodynamic temperature control as well as the correlated, competing, effects of non-temperature dependant processes, in this case biology, illustrated by the temperature corrected time series (Fig. 7 in red). Non-Redfield CO_2 draw-down (Schartau et al., 2007; Shadwick et al., 2010) counteracts the temperature driven changes in pCO_2 (Fig. 8). The spring and summer pCO_2 drawn-down occurs in the period of nutrient depletion, but is not necessarily resolved by the chlorophyll record. Furthermore, the SST coefficient likely comprises additional effects of changes in salinity, which are also anti-correlated with temperature. However, these salinity changes play only a minor role in changing pCO_2 (Fig. 8) due to the opposing effects of alkalinity and dissolved inorganic carbon on pCO_2 (Shadwick et al., 2010). The combined effects of temperature (with a SST coefficient of 16 to 18 µatm °C^{-1}),

BGD
7, 5269–5304, 2010

post-bloom biology and hydrographic changes (i.e. non-temperature effects with an SST coefficient of $-13\,\mu atm\,^{\circ}C^{-1}$), explain the deviation of the temperature coefficient from the thermodynamic prediction and the value of $4.6\,\mu atm\,^{\circ}C^{-1}$ obtained here. For frequencies shorter than $f = 0.007\,h^{-1}$, (periods longer than 6 days), the gain in pCO_2 due to SST in the in-situ data (Fig. 7, blue line) approaches the value of $4.6\,\mu atm\,^{\circ}C^{-1}$ obtained with the regression.

4 Results and discussion

The annual cycle of pCO_2 on the Scotian Shelf is dominated by the large seasonal amplitude of SST (Fig. 3a), with near 0 °C winter minimum, and summer maximum approaching 20 °C. The rapid and pronounced pCO_2 draw-down by the spring phytoplankton bloom in March or April is short-lived. The post-bloom recovery of pCO_2 is coincident with the warming of the surface waters, which acts to increase pCO_2. In autumn and winter the deepening of the mixed layer facilitates intrusion of CO_2-rich waters into the surface layer and damps the decrease of pCO_2 due to the cooling of surface waters. Overall, the surface waters of the Scotian Shelf act as a source of CO_2 to the atmosphere throughout most of the year (Figs. 11 and 3). A reversal of this trend generally occurs only during, and immediately following, the spring phytoplankton bloom when the waters become undersaturated with respect to the atmosphere (Fig. 3b and c).

The overall direction and inter-annual variability of the annual CO_2 fluxes are preconditioned by temperature and wind speed in the winter and, less significantly, in the late summer and autumn. This occurs primarily through the control of the depth of the winter mixed-layer, and thus the availability of nutrients to fuel the spring bloom (Fig. 9) (Greenan et al., 2008). A more detailed investigation of the years 2002, 2003 and 2005 serves to illustrate the governing mechanisms (see also Fig. 3). The winter of 2001/2002 had warmer minimum temperatures, and weaker winds than the 10-year average. This permitted an early onset of stratification with the initiation of the spring

BGD
7, 5269–5304, 2010

bloom beginning in March. Since mixing the previous winter was shallow, the bloom was inferred to be weak due to the reduced availability of nutrients from deeper waters. Following the weak bloom, strong late summer and autumn winds enhanced out-gassing in the second half of the year and yielded a large annual CO_2 flux to the atmosphere during 2002 (Fig. 3c). The winter of 2002/2003 had, in contrast, particularly cold minimum temperatures and strong winds resulting in a high degree of mixing; the 2003 spring bloom was therefore pre-conditioned with high nutrient concentrations which is reflected in the magnitude of the CO_2 uptake in March and April, and the reduction in annual CO_2 release to the atmosphere relative to the previous year. It is not only the winter conditions that control the expression of the spring bloom. For example, a comparably weak wind regime during spring 2005 permitted the bloom and the CO_2 undersaturation of the surface waters to persist from February through May. In addition, cold summer maximum temperature and weak autumn winds inhibited outgassing in the second half of the year, and resulted in weak CO_2 release during 2005 (Fig. 3).

The 10-year hindcast of pCO_2 and air-sea CO_2 fluxes reveals multi-annual to decadal trends in addition to the interannual variability (Fig. 3c). The SST anomaly reveals a decrease of 0.13 °C per year, or 1.3 °C over the 10-year period of computation. Simultaneously, the ΔpCO_2 ($\Delta pCO_2 = pCO_2^{Ocean} - pCO_2^{Atm}$), in which the anthropogenic atmospheric CO_2 increase has been explicitly included (Eq. 1), decreased by 2.3 µatm per year, or 23 µatm over the decade (Fig. 10). This decrease in the ΔpCO_2 anomaly can satisfactorily be explained by the observed temperature decrease. The thermodynamic temperature correction for pCO_2 results in a 4% change in pCO_2 for a 1 °C change in temperature (Takahashi et al., 2002). Applying this correction to the decadal mean pCO_2 (roughly 420 µatm), the observed decrease in temperature anomaly (0.13 °C per year) would account for a decrease in ΔpCO_2 of 2.2 µatm per year, as revealed by the ΔpCO_2 anomaly. The negative, or near neutral, North Atlantic Oscillation (NAO) index over the past decade is associated with an increased transport of cold Labrador Current Water onto the Scotian Shelf, and thus with anomalously cold waters in the region (Thompson and Wallace, 2001; Petrie, 2007; Thomas et al., 2008).

BGD
7, 5269–5304, 2010

The cooling of the water effectively shifts the position of the equilibrium ΔpCO_2 state, driving the system toward uptake. Conversely, warming of the water drives the system toward outgassing. Thus, while the interannual variability is controlled by local atmospheric forcing, (Fig. 9), the multi-annual to decadal changes appear to be controlled by larger scale hemispheric processes, in this case represented by the local expression of the NAO.

The satellite-based extrapolation of the pCO_2 algorithm to include the wider Scotian Shelf region allows the spatial variability in the region to be assessed (Fig. 11). From 1999–2008 the shelf integrated fluxes vary substantially between $-1.7\,\mathrm{mol\,C\,m^{-2}\,yr^{-1}}$ or ($-380\,\mathrm{Gmol\,C\,yr^{-1}}$, over the shelf area) and $-0.01\,\mathrm{mol\,C\,m^{-2}\,yr^{-1}}$ or ($-3.9\,\mathrm{Gmol\,C\,yr^{-1}}$, over the shelf area, see also Fig. 11 and Table 3). A gradient exists between the outflow of the Gulf of St. Lawrence at Cabot Strait, and the southwestern region in the Gulf of Maine. The Cabot Strait region has consistently weaker annual CO_2 release, and even acts in some years as a sink for CO_2. These waters exhibit the coldest (below freezing) winter temperatures and strongest spring blooms corresponding to the largest seasonal CO_2 uptake during the year. In contrast, the Gulf of Maine is warmer, and the spring bloom, and corresponding CO_2 uptake, is weaker. While particularly large CO_2 release is computed for 2000 and 2002 over the whole region (see also Fig. 3c), the general trend for the 10-year period is a weakening CO_2 release consistent with the decreasing trend in the ΔpCO_2 anomaly over the shelf (Fig. 10). The gradual change toward stronger CO_2 uptake on the Scotian shelf is in line with interpretations of the role of the NAO in controlling hydrographic patterns (Schuster and Watson, 2007; Thomas et al., 2008). However, consistent with suggestions of a longer-term decline in the CO_2 sink in the North Atlantic Ocean as a whole (Watson et al., 2009), we cannot presently exclude the possibility that long-term changes in North Atlantic circulation patterns would potentially cause similar trends due to a weakened northward, and strengthened southward, water transport (Bryden et al., 2005).

BGD
7, 5269–5304, 2010

Our findings indicate that the Scotian Shelf acts a source of CO_2, contrary to findings in many high-latitude continental shelf seas that act as net sinks for atmospheric CO_2 (Thomas et al., 2004; Chen and Borges, 2009). The East China Sea, an example of a continental shelf sea in the western Pacific, similar to the Scotian Shelf with respect to its location on the western side of the ocean basin under the influence of a northward flowing boundary current. The East China Sea has been well studied with respect to the inorganic carbon system (e.g., Tsunogai et al., 1997; Chen and Wang, 1999; Tsunogai et al., 1999; Wang et al., 2000). The East China Sea absorbes roughly twice as much CO_2 as is emitted annually from the Scotian Shelf region. The outgassing of CO_2 on the Scotian Shelf is primarily due to the competing effects of temperature and biology in the system, along with the late-autumn and winter destratification of the water column. The spring bloom on the Scotian Shelf results in a significant but brief CO_2 drawdown, and occurs at the temperature minimum. The decay of this bloom, and resulting production of CO_2 through the remineralization of organic matter is coincident with surface warming, which increases the pCO_2 to supersaturation with respect to the atmosphere. Continued biological production in the summer and early autumn is not sufficient to overcome this supersaturation. The water cools in late autumn, reducing pCO_2. Over the same period the water column becomes destratified and the region is subject to wind forcing, episodic upwelling (Petrie et al., 1987), and convective mixing, all three of which introduce carbon-rich waters from below the surface, maintaining the surface supersaturation until the following spring. The Scotian Shelf behaves similarly to an upwelling system, which are often biologically productive systems which release CO_2 to the atmosphere due to the delivery of DIC-rich waters from below (Lendt et al., 2003; Thomas et al., 2005). By contrast, the North Sea, which acts a sink for atmospheric CO_2 of roughly the same magnitude as the Scotian Shelf (Thomas et al., 2005), could be classified as a downwelling system (Huthnance et al., 2009). It has been suggested that the downwelling circulation in the North Sea promotes the transport of dissolved inorganic carbon off the shelf to the deep ocean facilitating the uptake of atmospheric CO_2 in the subsequent productive season (Huthnance et al., 2009).

BGD
7, 5269–5304, 2010

This observation-based approach to understand the dynamics of the CO_2 system on the Scotian Shelf (see also Shadwick et al., 2010) yields conflicting results to modelling studies of the same region (Fennel et al., 2008; Previdi et al., 2009). However, our approach produces results in agreement with a similar process study in the neighboring Gulf of Maine (Vandemark et al., 2010). Previdi et al. (2009) have suggested that interannual variability in air-sea CO_2 flux on the eastern North American continental shelf is due in part to NAO forcing. They suggest that warming between (low NAO) 1985 and (high NAO) 1990 drove the system in the Gulf of Maine towards weaker uptake; this interpretation is agreement with our finding that the decadal cooling on the Scotian Shelf has driven the system towards stronger uptake. The reasons for the discrepancy betwen the observation- and model-based approaches is currently unknown and is beyond the scope of this study.

5 Conclusions

High frequency in-situ time-series observations deepen our understanding of individual regional characteristics of the CO_2 system particularly in coastal regions, where temporal and spatial variability is high. This allows reliable relationships between pCO_2 and remotely sensed variables to be established and understood. Coupled to such in-situ observations, the application of satellite data has the potential to improve the understanding and assessment of air-sea CO_2 fluxes in the coastal ocean, which, as shown here, can vary by two orders of magnitude at interannual to decadal times scales.

Acknowledgements. We thank R. Davis for his assistance with the CARIOCA data processing, K. Thompson and J. Cullen for assistance with the statistical analysis and in-depth comments on the manuscript, and D. Worthy at Environment Canada for providing the atmospheric CO_2 data. We are grateful to J. Barthelotte, M. Scotney, and B. Greenan for the deployment and recovery of the CARIOCA buoy, and to J. Spry and the Bedford Institute of Oceanography for making the archived data from station HL2 accessible. This work was supported by the National Science and Engineering Research Council of Canada, the Canadian Foundation for Climate

BGD
7, 5269–5304, 2010

and Atmospheric Sciences, the National Science Foundation, NASA, and by MetOcean Data Systems. This work contributes to IGPB/IHDP-LOICZ.

References

Bakker, D. C. E., Etcheto, J., Boutin, J., and Merlivat, L.: Variability of surface water fCO_2 during seasonal upwelling in the equatorial Atlantic Ocean as observed by adrifting buoy, J. Geophys. Res., 106, 9241–9253, 2001. 5272

Banse, K.: Zooplankton: pivotal role in the control of ocean production, ICES J. Mar. Sci., 52, 265–277, 1995. 5277

Bates, N. R., Merlivat, L., Beaumont, L., and Pequignet, A. C.: Intercomparison of shipboard and moored CARIOCA buoy seawater fCO_2 measurements in the Sargasso Sea, Mar. Chem., 72, 239–255, 2000. 5272

Borges, A. V., Tilbrook, B., Metzl, N., Lenton, A., and Delille, B.: Inter-annual variability of the carbon dioxide oceanic sink south of Tasmania, Biogeosciences, 5, 141–155, doi:10.5194/bg-5-141-2008, 2008. 5271

Boutin, J. and Merlivat, L.: New in-situ estimates of carbon biological production rates in the Southern Ocean from CARIOCA drifter measurements, Geophys. Res. Lett., 36, L13608, doi:10.1029/2009GL038307, 2009. 5270

Bryden, H. L., Longworth, H. R., and Cunningham, S. A.: Slowing of the Atlantic meridional overturning circulation at 25° N, Nature, 438, 655–657, 2005. 5283

Cai, W.-J., Dai, M. H., and Wang, H. C.: Air-sea exchange of carbon dioxide in ocean margins: A province-based synthesis, Geophys. Res. Lett., 33, L12603, doi:10.1029/2006GL026219, 2006. 5271

Chen, C.-T. A. and Borges, A. V.: Reconciling opposing views on carbon cycling in the coastal ocean: Continental shelves as sinks and near-shore ecosystems as sources of atmospheric CO_2, Deep-Sea Res. Pt. II, 33, L12603, doi:10.1016/j.dsr2.2009.01.001, 2009. 5284

Chen, C. T.-A. and Wang, S. L.: Carbon, alkalinity and nutrient budget on the East China Sea continental shelf, J. Geophys. Res., 104, 20675–20686, 1999. 5284

Chierici, M., Olsen, A., Johannessen, T., Trinanes, J., and Wanninkhof, R.: Algorithms to estimate the carbon dioxide uptake in the northern North Atlantic using shipboard observations, satellite and ocean analysis data, Deep-Sea Res., 56, 630–639, 2009. 5271, 5276

BGD

7, 5269–5304, 2010

Copin-Montégut, C., Bégovic, M., and Merlivat, L.: Variability of the partial pressure of CO_2 on diel to annual time scales in the Northwestern Mediterranean Sea, Mar. Chem., 85, 169–189, 2004. 5272

Etcheto, J., Boutin, J., Dandonneau, Y., Bakker, D. C. E., Feely, R. A., Ling, R. D., Nightingale, P. D., and Wanninkhof, R.: Air-sea CO_2 flux variablity in the equatorial Pacific Ocean near 100° W, Tellus B, 51, 734–737, 1999. 5271

Fennel, K., Wilkin, J., Previdi, M., and Najjar, R.: Denitrification effects on air-sea CO_2 flux in the coastal ocean: Simulations for the northwest North Atlantic, Geophys. Res. Lett., 35, L24608, doi:10.1029/2008GL036147, 2008. 5285

Greenan, B. J. W., Petrie, B. D., Harrison, W. G., and Strain, P. M.: The onset and evolution of aspring bloom on the Scotian Shelf, Limnol. Oceanogr., 53, 1759, doi:10.1029/2008GL036147, 2008. 5281

Huthnance, J. M., Holt, J. T., and Wakelin, S. L.: Deep ocean exchange with west-European shelf seas, Ocean Sci., 5, 621–634, doi:10.5194/os-5-621-2009, 2009. 5284

Kiefer, D. A.: Fluorescence Properties of Natural Phytoplankton Populations, Mar. Biol., 22, 263–269, 1973. 5272

Körtzinger, A., Thomas, H., Schneider, B., Gronau, N., Mintrop, L., and Duinker, J. C.: At-sea intercomparison of two newly designed underway pCO_2 systems – encouraging results, Mar. Chem., 52, 133–145, 1996. 5274

Lefèvre, N., Aiken, J., Rutllant, J., Daneri, G., Lavender, S., and Smyth, T.: Observations of pCO_2 in the coastal upwelling off Chile: Spatial and temporal extrapolation using satellite data, J. Geophys. Res., 107, 3055, doi:10.1029/2000JC000395, 2002. 5271

Lefévre, N., Guillot, A., Beaumont, L., and Danguy, T.: Variability of fCO_2 in the Eastern Tropical Atlantic from a moored buoy, J. Geophys. Res., 113, C01015, doi:10.1029/2007JC004146, 2008. 5271

Lendt, R., Thomas, H., Hupe, A., and Ittekkot, V.: Response of the near-surface carbonate system of the northwestern Arabian Sea to the southwest monsoon and related biological forcing, J. Geophys. Res., 108, 3222, doi:10.1029/2000JC000771, 2003. 5284

Lewis, E. and Wallace, D. W. R.: Program Developed for CO_2 Systems Calculations, ORNL/CDIAC 105, Carbon Dioxide Information Analysis Center, Oak Ridge National Laboratory US Department of Energy, Oak Ridge, Tennessee, 1998. 5275

Lohrenz, S. E. and Cai, W.-J.: Satellite ocean color assessment of air-sea fluxes of CO_2 in ariver-dominated coastal margin, Geophys. Res. Lett., 33, L01601,

BGD
7, 5269–5304, 2010

doi:10.1029/2005GL023942, 2006. 5271
Naegler, T., Ciais, P., Rodgers, K., and Levin, I.: Excess radiocarbon constraints on air-sea gas exchange and the uptake of CO_2 by the oceans, Geophys. Res. Lett., 33, L11802, doi:10.1029/2005GL025408, 2006. 5276
Olsen, A., Brown, K. R., Chierici, M., Johannessen, T., and Neill, C.: Sea-surface CO_2 fugacity in the subpolar North Atlantic, Biogeosciences, 5, 535–547, doi:10.5194/bg-5-535-2008, 2008. 5271
Padin, X. A., Castro, C. G., Rios, A. F., and Pérez, F. F.: fCO_2^{sw} variability in the Bay of Biscay during ECO cruises, Cont. Shelf Res., 28, 904–914, 2008. 5271
Petrie, B.: Does the North Atlantic Oscillation affect hydrographic properties on the Canadian Atlantic continental shelf? Atmos. Ocean, 45, 141–151, 2007. 5282
Petrie, B. and Smith, P. C.: Low-frequency motions on the Scotian shelf and slope, Atmosphere, 15, 117–140, 1977. 5276
Petrie, B., Topliss, B. J., and Wright, D. G.: Coastal upwelling and eddy development off nova scotia, J. Geophys. Res., 29, 12979–12991, 1987. 5284
Platt, T., Bird, D., and Sathyendranath, S.: Critical depth and marine primary production, P. R. Soc. Lond. B Bio., 246, 205–217, 1991. 5277
Previdi, M., Fennel, K., Wilkin, J., and Haidvogel, D.: Interannual variability in atmospheric CO_2 uptake on the northeast US continental shelf, J. Geophys. Res., 114, G04003, doi:10.1029/2008JG000881, 2009. 5285
Sabine, C. L., Feely, R. A., Gruber, N., Key, R. M., Lee, K., Bullister, J. L., Wanninkhof, R., Wong, C. S., Wallace, D. W. R., Tilbrook, B., Millero, F. J., Peng, T.-H., Kozyr, A., Ono, T., and Rios, A. F.: The Oceanic Sink for Anthropogenic CO_2, Science, 305, 367–371, 2004. 5270
Salisbury, J. E., Vandemark, D., Hunt, C. W., Campbell, J. W., McGillis, W. R., and McDowell, W. H.: Seasonal observations of surface waters in two Gulf of Maine estuary-plume systems: relationships between watershed attributes, optical measurements and surface pCO_2, Estuar. Coast. Shelf S., 77, 245–252, 2008. 5271
Schartau, M., Engel, A., Schröter, J., Thoms, S., Völker, C., and Wolf-Gladrow, D.: Modelling carbon overconsumption and the formation of extracellular particulate organic carbon, Biogeosciences, 4, 433–454, doi:10.5194/bg-4-433-2007, 2007. 5280
Schuster, U. and Watson, A. J.: A variable and decreasing sink for atmospheric CO_2 in the North Atlantic, J. Geophys. Res., 112, C11006, doi:10.1029/2006JC003941, 2007. 5271, 5283

BGD
7, 5269–5304, 2010

Schuster, U., Watson, A. J., Bates, N. R., Corbière, A., Gonzalez-Davila, M., Metzl, N., Pierrot, D., and Santana-Casiano, M.: Trends in North Atlantic sea-surface fCO_2 from 1990 to 2006, Deep-Sea Res. Pt. II, 56, 620–629, 2009. 5271

Shadwick, E. H., Thomas, H., Azetsu-Scott, K., Greenan, B. J. W., Head, E., and Horne, E.: Seasonal variability of dissolved inorganic carbon and surface water pCO_2 in the Scotian Shelf region of the Northwestern Atlantic, Mar. Chem., under revision, 2010. 5275, 5276, 5280, 5301

Sweeney, C., Gloor, E., Jacobson, A. R., Key, R. M., McKinley, G., Sarmiento, J. L., and Wanninkhof, R.: Constraining global air-sea gas exchange for CO_2 with recent bomb ^{14}C measurements, Global Biogeochem. Cy., 21, GB2015, doi:10.1029/2006GB002784, 2007. 5276

Takahashi, T., Sutherland, S. C., Sweeney, C., Poisson, A., Metzl, N., Tilbrook, B., Bates, N. R., Wanninkhof, R., Feely, R. A., Sabine, C. L., Olafsson, J., and Nojiri, Y.: Global sea-air CO_2 flux based on climatological surface ocean pCO_2, and seasonal biological and temperature effects, Deep-Sea Res. Pt. II, 49, 1601–1622, 2002. 5277, 5279, 5282

Takahashi, T., Sutherland, S. C., Wanninkhof, R., Sweeney, C., Feely, R. A., Chipman, D. W., Hales, B., Friederich, G., Chavez, F., Sabine, C., Watson, A., Bakker, D. C., Schuster, U., Metzl, N., Yoshikawa-Inoue, H., Ishii, M., Midorikawa, T., Nojiri, Y., Körtzinger, A., Steinhoff, T., Hoppema, M., Olafsson, J., Arnarson, T. S., Tilbrook, B., Johannessen, T., Olsen, A., Bellerby, R., Wong, C., Delille, B., Bates, N., and de Baar, H. J.: Climatological mean and decadal changes in surface ocean pCO_2, and net sea-air CO_2 flux over the global oceans, Deep-Sea Res. Pt. II, 56, 554–577, 2009. 5270

Taylor, A. H., Geider, R. J., and Gilber, F. J. H.: Seasonal and latitudinal dependencies of phytoplankton carbon-to-chlorophyll a ratios: results of a modelling study, Mar. Ecol.-Prog. Ser., 152, 51–66, 1997. 5277

Thomas, H., Bozec, Y., Elkalay, K., and de Baar, H. J. W.: Enhanced open ocean storage of CO_2 from shelf sea pumping, Science, 304, 1005–1008, 2004. 5271, 5284

Thomas, H., Bozec, Y., Elkalay, K., de Baar, H. J. W., Borges, A. V., and Schiettecatte, L.-S.: Controls of the surface water partial pressure of CO_2 in the North Sea, Biogeosciences, 2, 323–334, doi:10.5194/bg-2-323-2005, 2005. 5284

Thomas, H., Prowe, A. E. F., van Heuven, S., Bozec, Y., de Baar, H. J. W., Schiettecatte, L.-S., Suykens, K., Koné, M., Borges, A. V., Lima, I. D., and Doney, S. C.: Rapid decline of the CO_2 buffering capacity in the North Sea and implications for the North Atlantic Ocean, Global Biogeochem. Cy., 21, GB4001, doi:10.1029/2006GB002825, 2007. 5271

BGD
7, 5269–5304, 2010

Thomas, H., Prowe, F., Lima, I. D., Doney, S. C., Wanninkhof, R., Greatbatch, R. J., Schuster, U., and Corbière, A.: Changes in the North Atlantic Oscillation influence CO_2 uptake in the North Atlantic over the past 2 decades, Global Biogeochem. Cy., 22, GB4027, doi:10.1029/2007GB003167, 2008. 5271, 5273, 5282, 5283

Thompson, D. W. and Wallace, J. M.: Regional climate impacts of the Northern Hemisphere annular mode, Science, 293, 85–89, 2001. 5282

Tsunogai, S., Watanabe, S., Nakamura, S., Ono, T., and Sato, T.: A preliminary study of carbon system in teh East China Sea, J. Oceangr., 53, 9–17, 1997. 5284

Tsunogai, S., Watanabe, S., and Sato, T.: Is there a "continental shelf pump" for the absorption of atmospheric CO_2?, Tellus, 51, 701–712, 1999. 5271, 5284

Umoh, J. U. and Thompson, K. R.: Surface heat flux, horizontal advection, and the seasonal evolution of water temperature on the Scotian Shelf, J. Geophys. Res., 99, 20403–20416, 1994. 5279

Vandemark, D., Salisbury, J. E., Hunt, C. W., Shellito, S., and Irish, J.: Temporal and spatial dynamics of CO_2 air-sea flux in the Gulf of Maine, J. Geophys. Res., submitted, 2010. 5285

Wang, S. L., Chen, C. T. A., Hong, G. H., and Chung, C. S.: Carbon dioxide and related parameters in the East China Sea, Cont. Shelf Res., 20, 525–544, 2000. 5284

Wanninkhof, R.: Relationships between wind speed and gas exhange over the ocean, J. Geophys. Res., 97, 7373–7382, 1992. 5272, 5276

Wanninkhof, R., Olsen, A., and Trinanes, J.: Air-sea CO_2 fluxes in the Caribbean Sea from 2002–2004, J. Mar. Syst., 66, 272–284, 2007. 5271

Watson, A. J., Schuster, U., Bakker, D. C. E., Bates, N. R., Corbiére, A., González-Dávila, M., Friedrich, T., Hauck, J., Heinze, C., Johannessen, T., Körtzinger, A., Metzl, N., Olafsson, J., Olsen, A., Oschlies, A., Padin, X. A., Pfeil, B., Santana-Casiano, J. M., Steinhoff, T., Telszewski, M., Rios, A. F., Wallace, D. W. R., and Wanninkhof, R.: Tracking the variable North Atlantic sink for atmospheric CO_2, Science, 326, 1391–1393, 2009. 5270, 5276, 5283

Weeks, A., Conte, M. H., Harris, R. P., Bedo, A., Bellan, I., Burkill, P. H., Edwards, E. S., Harbour, D. S., Kennedy, H., and Llewellyn, C.: The physical and chemical environment and changes in community structure associated with bloom evolution: the JGOFS North Atlantic Bloom Experiment, Deep-Sea Res. Pt. II, 40, 347–368, 1993. 5277

Weiss, R. F.: Carbon dioxide in water and seawater: The solubility of a non-ideal gas, Mar. Chem., 2, 203–215, 1974. 5276

BGD
7, 5269–5304, 2010

Table 1. Notation for different time-series of chlorophyll-*a*.

Symbol	Description
F_{Chl}	chlorophyll-*a* fluorescece determined by fluorometer
Chl-*a*	discrete chlorophyll-*a* determined by extraction
Chl_F	fluorescence-derived chlorophyll-*a* used in Eq. (1)
Chl_{SAT}	satellite derived chlorophyll-*a* concentration

BGD
7, 5269–5304, 2010

Table 2. Non-standardized, or "B" regression coefficients (see Eq. 1) and the normalized, β coefficients.

	Chl_F	SST	k
B	−24.6	4.6	3.7
β	−0.65	0.50	0.25

BGD
7, 5269–5304, 2010

Table 3. The annual air-sea CO_2 fluxes from 1999 to 2008, both shelf-wide, and in Box 1 containg the CARIOCA moorning, in units of mol C m^{-2} yr^{-1}. Negative values indicate an outgassing of CO_2 to the atmosphere. The 7 gird boxes covering the Scotian Shelf region have an area of 222 700 km^2; Box 1 has an area of 31 800 km^2 (see also Fig. 11).

	1999	2000	2001	2002	2003	2004	2005	2006	2007	2008
Shelf-wide	−0.6	−1.3	−0.7	−1.7	−0.8	−1.1	−0.5	−0.02	−0.1	−0.1
Box 1	−1.75	−2.25	−1.4	−2.45	−1.5	−1.5	−1.0	−0.8	−0.95	−1.1

BGD
7, 5269–5304, 2010

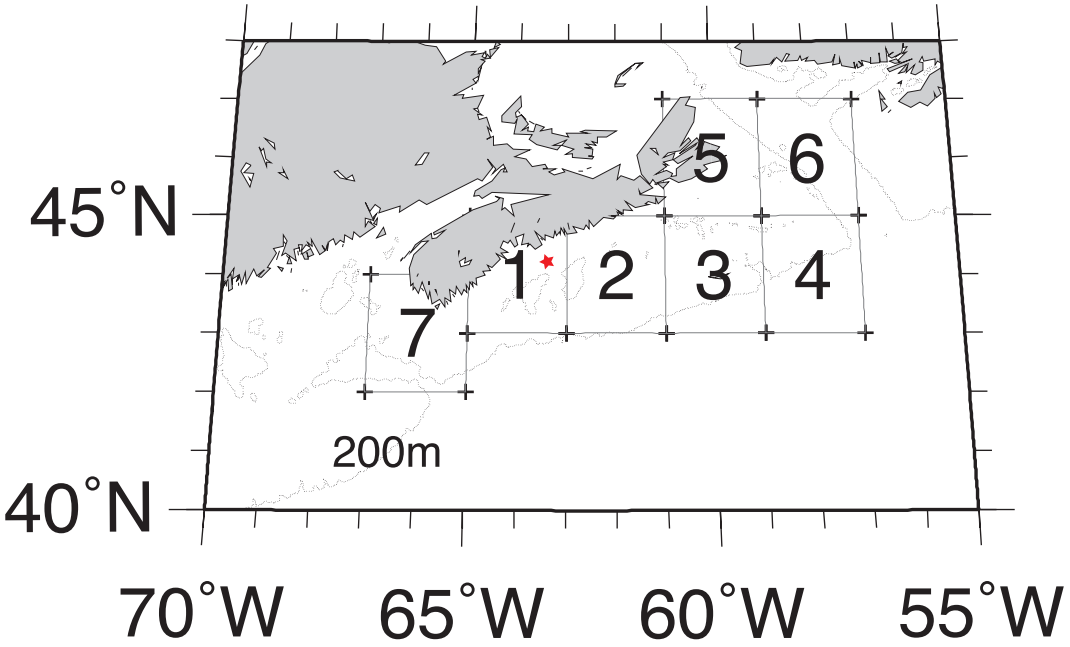

Fig. 1. The investigation is extrapolated spatially to include seven 2°×2° grid boxes covering the entire Scotian Shelf region (222 700 km^2). The CARIOCA buoy (red star) was moored at 44.3° N, 63.3° W, within box 1.

BGD
7, 5269–5304, 2010

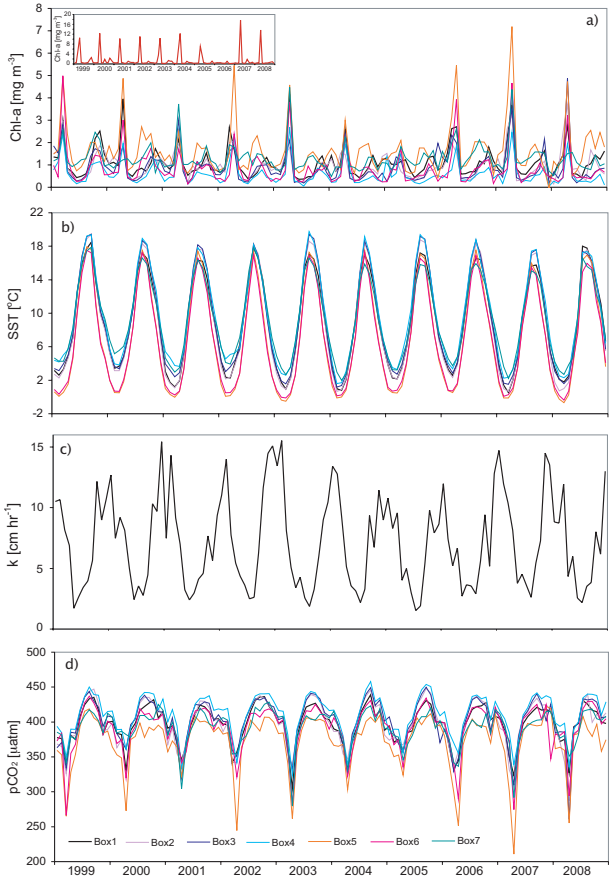

Fig. 2. (a) Chl_{SAT}, inset: discrete Chl-*a* data from monthly shipboard occupations of the CARIOCA mooring location. These data are not monthly means, but once-per month occupations expressly biased to record the spring chlorophyll maximum at the mooring site. **(b)** SST, **(c)** gas transfer velocity (*k*) and **(d)** computed pCO_2. For the locations of the grid boxes see Fig. 1.

BGD
7, 5269–5304, 2010

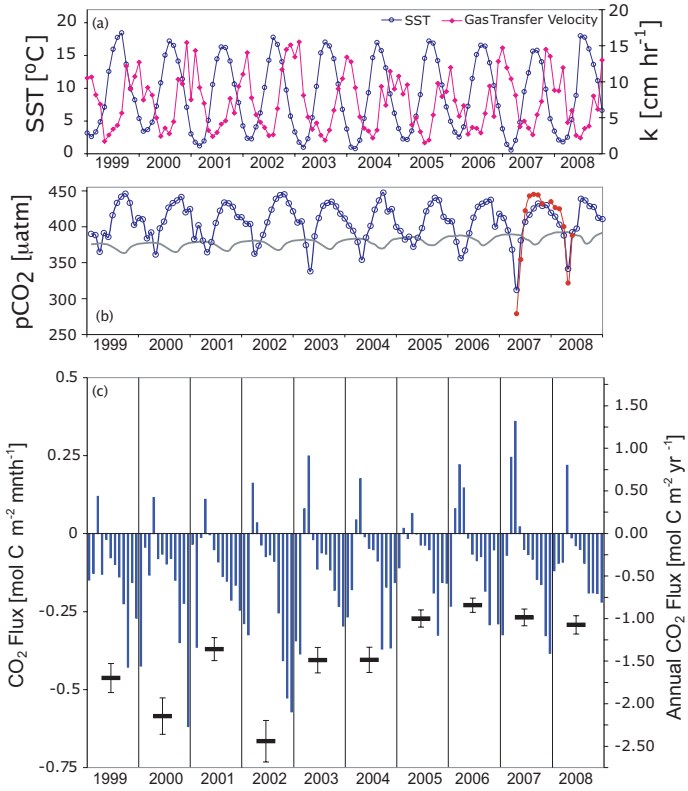

Fig. 3. **(a)** SST (blue line open symbols) and gas transfer velocity (pink line, closed symbols) for the 10-year period. **(b)** Computed surface water pCO_2 (Eq. 1) for the box comprising the mooring station (box1, see Fig. 1) (thick blue line with symbols). The computed values are compared to in-situ observations from 2007 and 2008 (in red). The solid gray line gives the monthly atmospheric CO_2 concentration. **(c)** The monthly CO_2 fluxes (vertical lines, left hand side y-axis) and integrated annual CO_2 fluxes (horizontal lines, right hand side y-axis)

BGD
7, 5269–5304, 2010

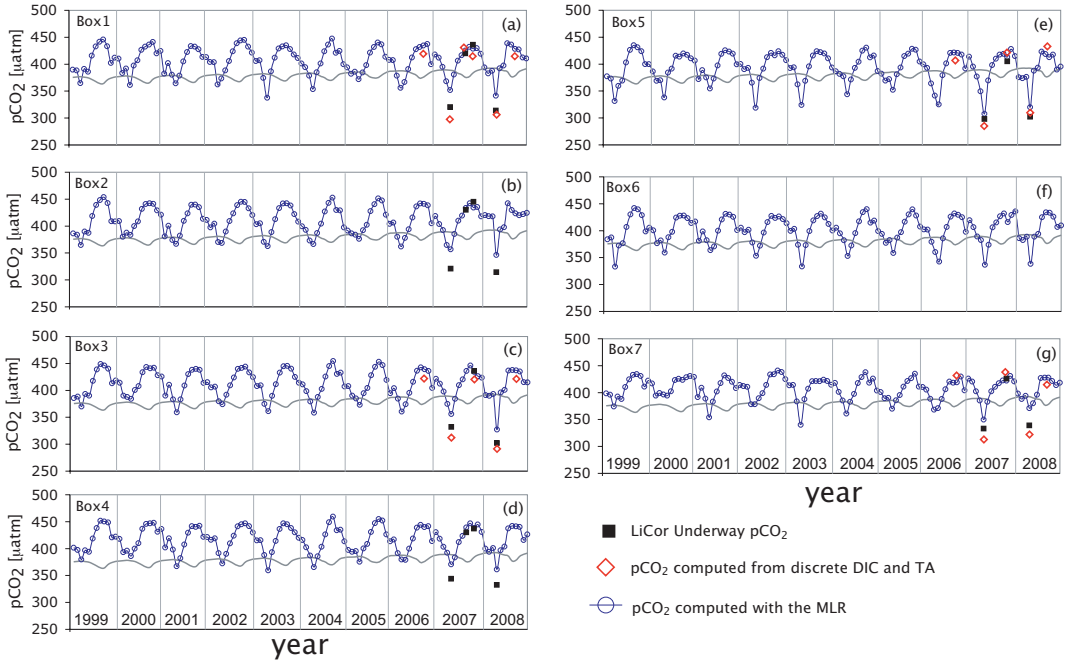

Fig. 4. The pCO_2 computed with Eq. (1) (blue line with symbols) is validated against two independent time-series of observations. The black squares indicate pCO_2 measurements made by an underway system, and the open red diamonds indicate pCO_2 computed from discret samples of DIC and TA. For the locations of the grid boxes (see Fig. 1).

BGD
7, 5269–5304, 2010

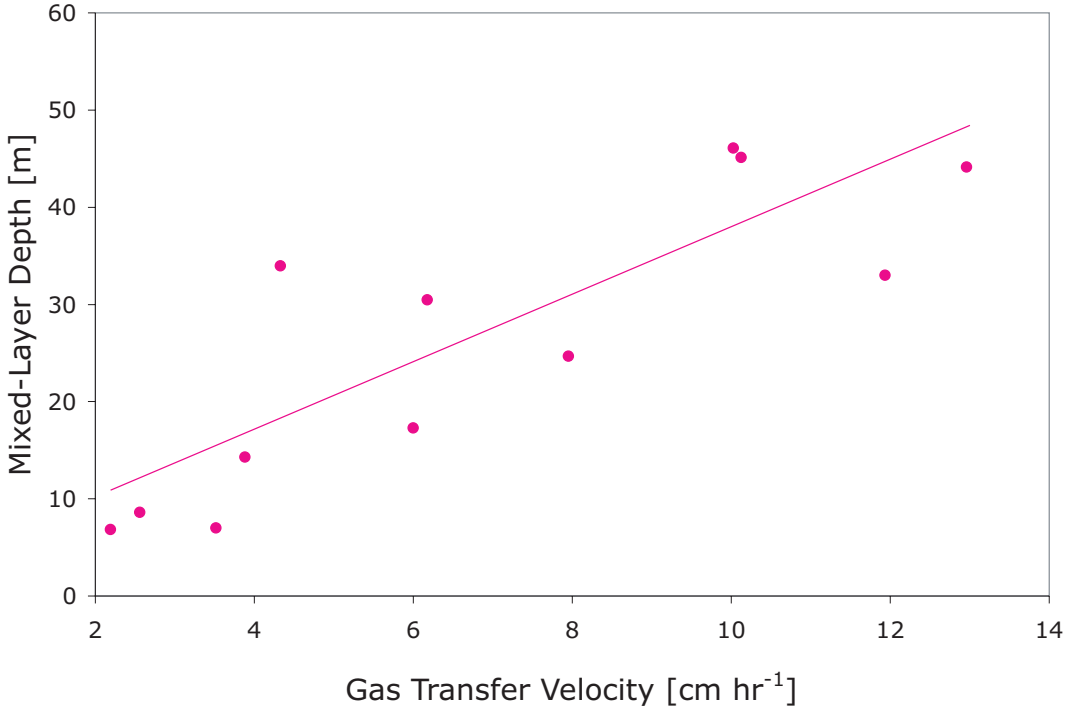

Fig. 5. The relationship between mixed-layer depth and gas transfer velocity. Mixed-layer depth is estimated from monthly profiles of temperature and salinity measured at the same location as the CARIOCA mooring (see Fig. 1).

BGD
7, 5269–5304, 2010

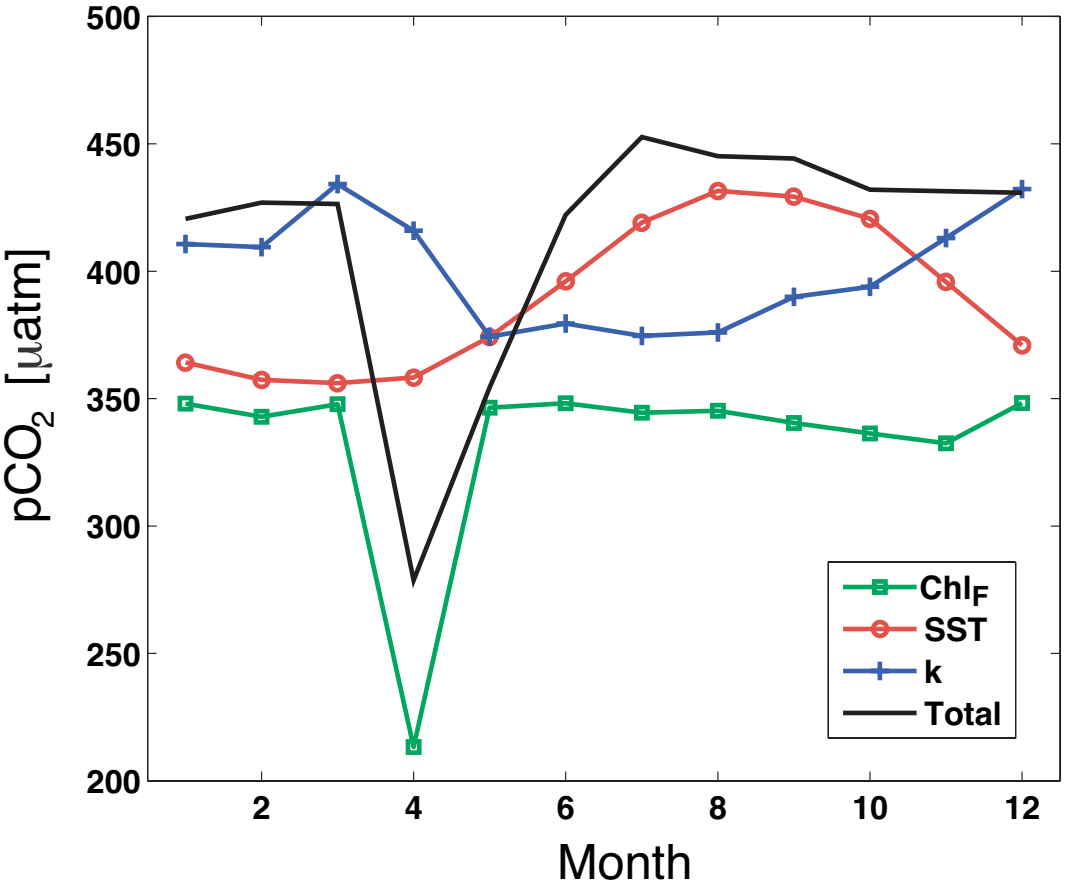

Fig. 6. The respective contributions from Chl_F (in green), SST (in red) and k (in blue) to the total change in pCO_2 (black) over the annual cycle.

BGD
7, 5269–5304, 2010

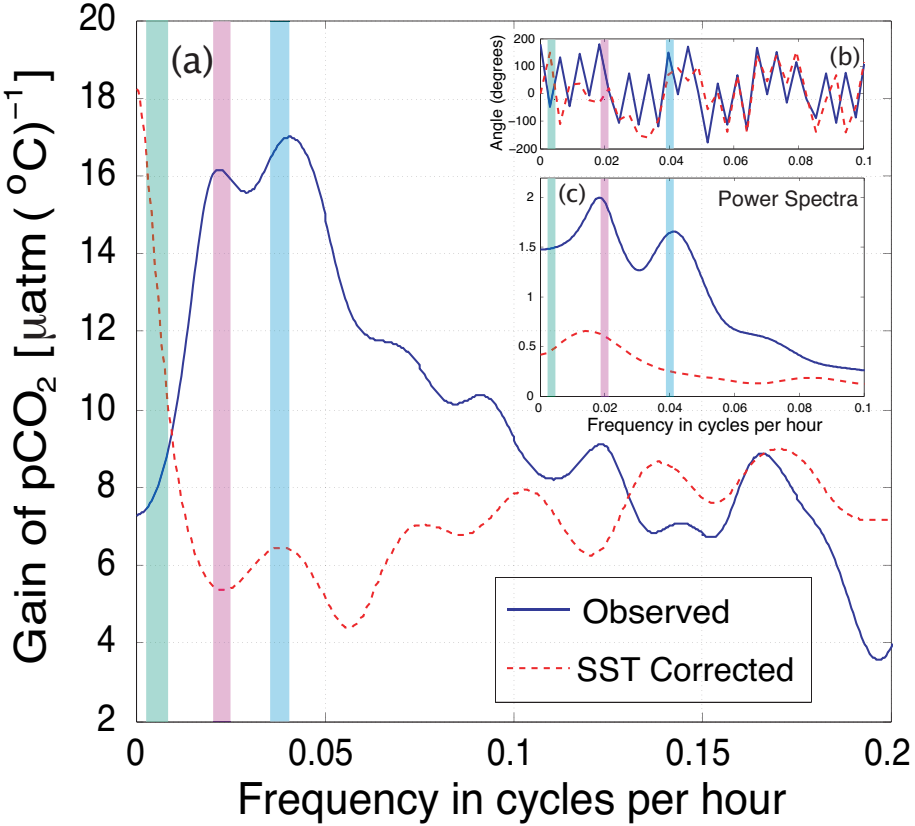

Fig. 7. **(a)** The gain of pCO_2 due to SST using the in-situ hourly data (blue), and the gain of pCO_2^* due to SST* (red dashed). Frequencies of $f = 0.04\,h^{-1}$, or 24-h (blue bar), $f = 0.02\,h^{-1}$ or roughly 40 h (pink bar), and $f = 0.007\,h^{-1}$ or 6 days (green bar) are indicated. **(b)** The phase spectra for the in-situ pCO_2 (blue line) and pCO_2^* (red dashed line) series. **(c)** The power spectra for the in-situ pCO_2 (blue) and pCO_2^* series (red dashed). The in-situ data is dominated by the 24-h cycle of SST, while the pCO_2^* series is dominated over longer time scales.

BGD
7, 5269–5304, 2010

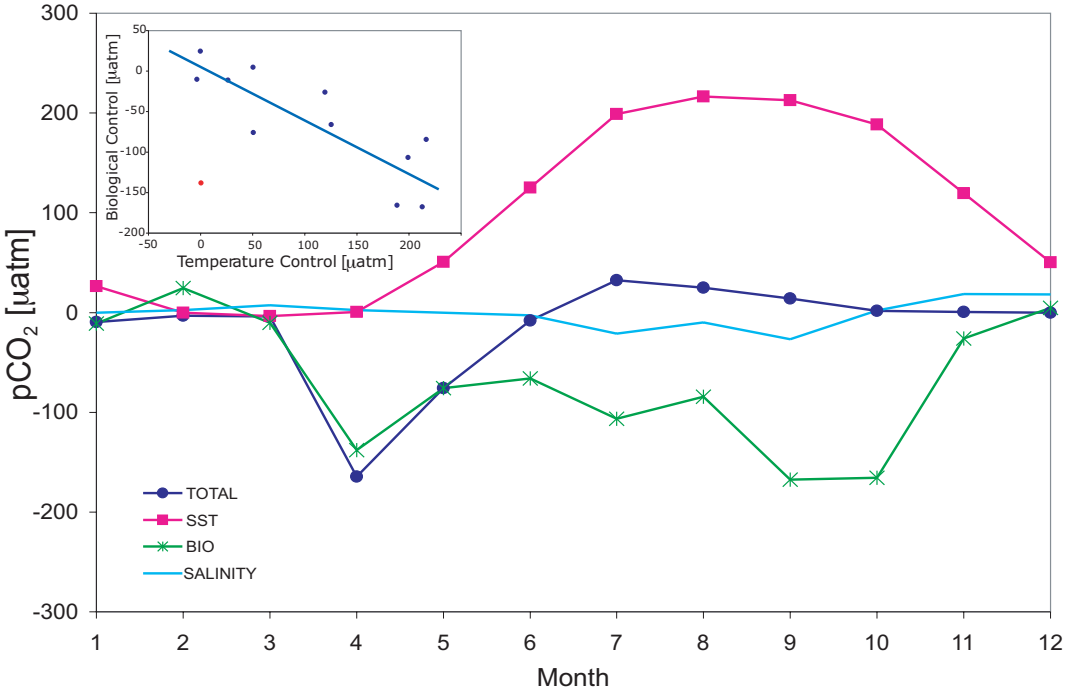

Fig. 8. The controls on surface water pCO_2 on the Scotian Shelf following Shadwick et al. (2010); values of pCO_2 are cumulative, relative to January. The effect of temperature (pink squares), biology (green asterisk), and salinity (blue line) are shown. Inset: The relationship between the temperature (pink squares) and biological (green asterisk) control. The linear regression line does not include the point indicated by the red asterisk, which is from the month of April, since it is clearly covered by the chlorophyll-*a* signal from the spring bloom.

BGD
7, 5269–5304, 2010

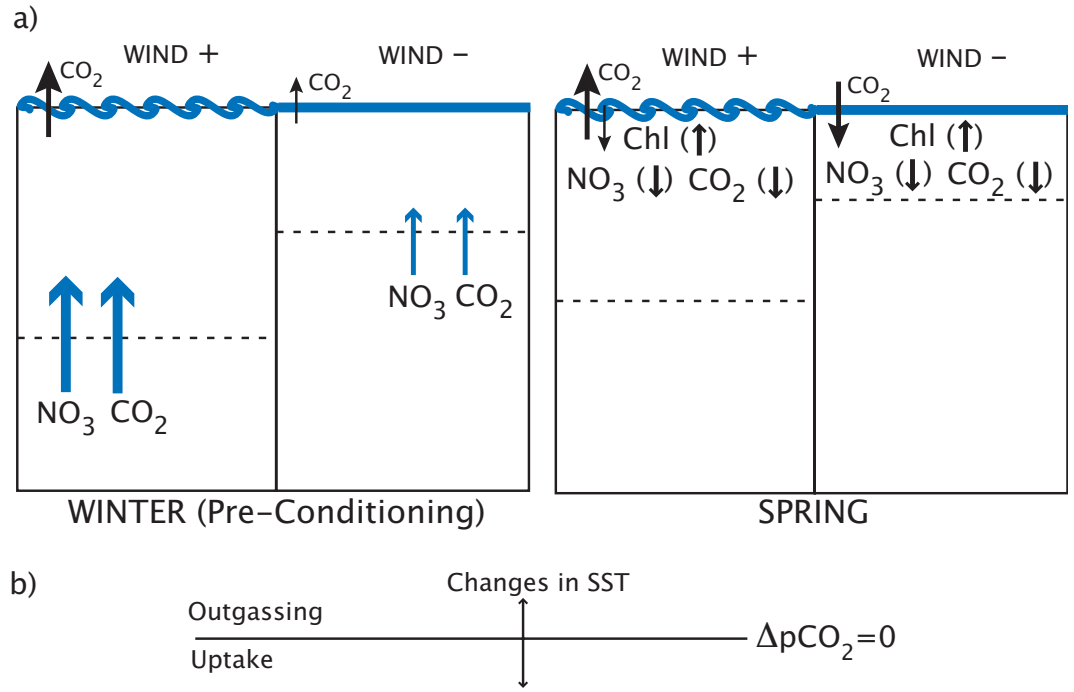

Fig. 9. A schematic representation of the processes controlling the interannual **(a)** and long-term **(b)** variability of the air-sea CO_2 fluxes in the system. (a) Uptake of CO_2 by the ocean occurs if the depletion of CO_2 by the phytoplankton bloom causes the undersaturation of the surface waters with respect to the atmosphere. (b) The long-term variability is controlled by larger scale hemispheric processes which determine the position of the ΔpCO_2 equilibrium state through surface water temperature.

BGD
7, 5269–5304, 2010

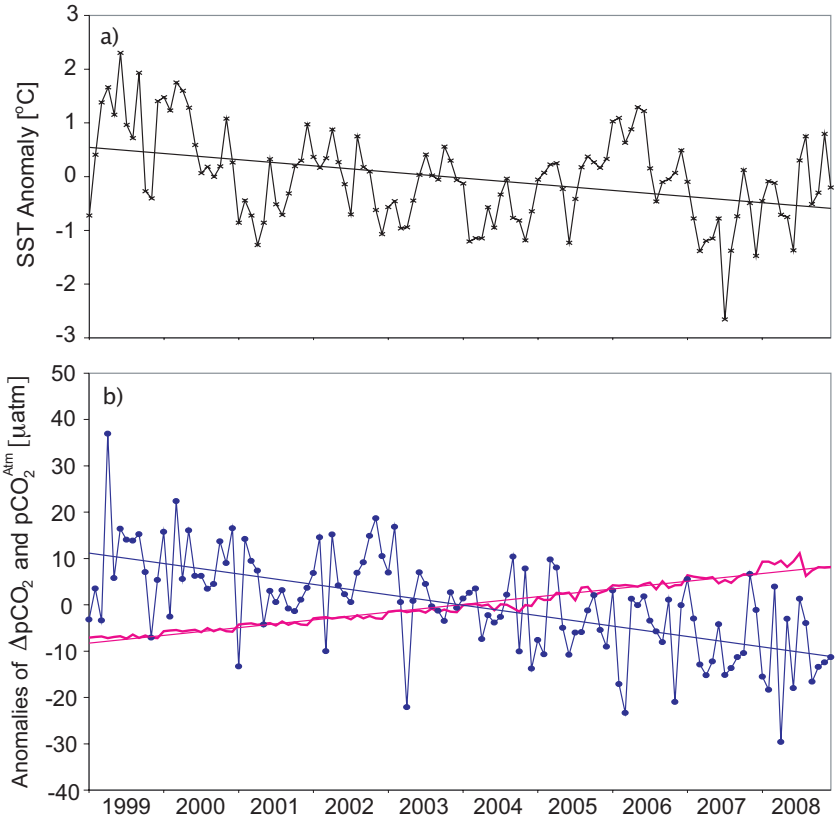

Fig. 10. Anomalies of **(a)** SST, and **(b)** ΔpCO_2 (blue circles) and atmospheric pCO_2 (pink solid line). The slope of SST linear regression line (solid black line) corresponds to a cooling of roughly 1.3 °C yr^{-1}. The slope of the atmospheric CO_2 anomaly (bold pink line) is roughly 1.7 µatm per year, in line with the annual increase due to anthropogenic emissions. The slope of the ΔpCO_2 anomaly (solid blue line) is −2.3 µatm per year, or −23 µatm over the decade.

BGD
7, 5269–5304, 2010

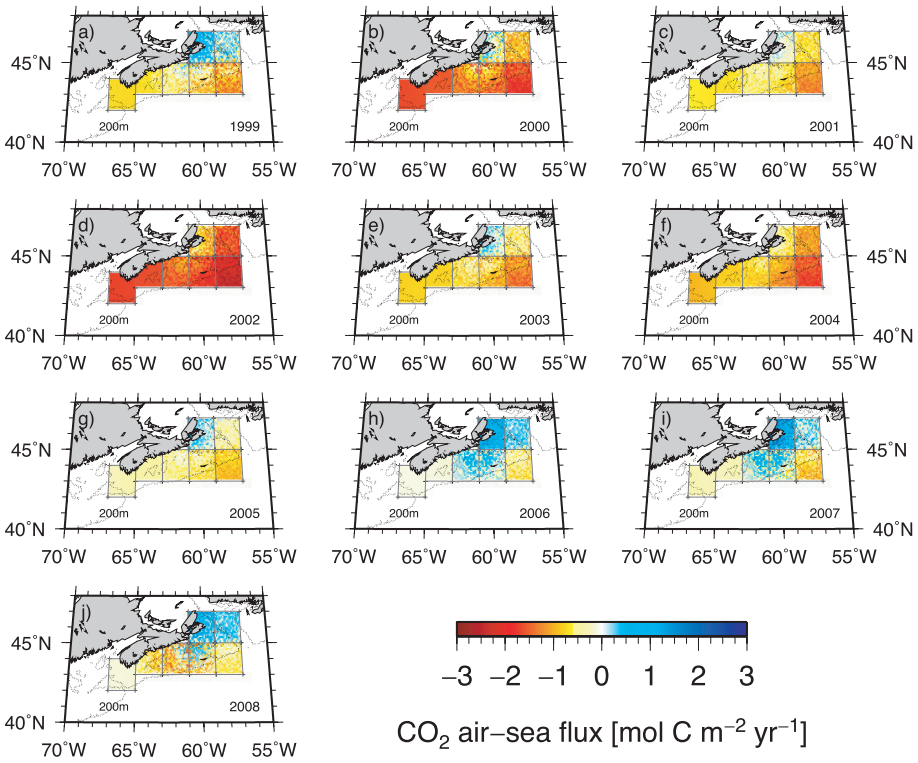

Fig. 11. The investigation is extrapolated spatially to include the entire Scotian Shelf region (222 700 km^2). The integrated annual air-sea CO_2 fluxes from 1999 (top left) to 2008 (bottom left) are shown. The annual, shelf-wide fluxes are: **(a)**, -0.6 mol C m^{-2} yr^{-1} (1999), **(b)** -1.3 mol C m^{-2} yr^{-1} (2000), **(c)**, -0.7 mol C m^{-2} yr^{-1} (2001), **(d)** -1.7 mol C m^{-2} yr^{-1} (2002), **(e)** -0.8 mol C m^{-2} yr^{-1} (2003), **(f)** -1.1 mol C m^{-2} yr^{-1} (2004), **(g)** -0.5 mol C m^{-2} yr^{-1} (2005), **(h)** -0.02 mol C m^{-2} yr^{-1} (2006), **(i)** -0.1 mol C m^{-2} yr^{-1} (2007) and **(j)** -0.1 mol C m^{-2} yr^{-1} (2008). Negative values indicate CO_2 release to the atmosphere.

BGD
7, 5269–5304, 2010